Geometry-Based UAV MIMO Channel Modeling and Pattern Optimization for Multimode Antennas

Nils Lennart Johannsen, Sami Alkubti Almasri, and Peter Adam Hoeher, *Fellow, IEEE*

***Abstract*— Improving safety is of general interest in aviation. Flight transponders used in collision avoidance systems advise pilots with information of potential collisions and avoidance resolutions. Some transponders are capable of transmitting the instantaneous position of the vehicle which might be turned off. To prevent autonomous flights from collisions, the transponder signals shall be used to estimate the direction-of-arrival (DoA). Recently, multimode antennas have been investigated for communication and localization purposes. Multimode antennas provide several orthogonal ports on a single radiator surface. This leads to a reduction of space and weight, which is of interest in airborne applications. To perform DoA estimation as well as communication, a suitable channel model is required. In this contribution, a channel model fulfilling the requirements for both multiple-input multiple-output (MIMO) communication and DoA estimation is proposed. This channel model relies on the manifold matrix representation of the UAV under consideration. The derived description of a manifold matrix for the UAV use-case is used for an optimization to achieve a close to omnidirectional radiation pattern. Therefore, different optimization functions are derived and their performance is compared. The results of the optimization using the calculated manifold matrix are verified by measurements taken in an antenna measurement chamber.**

***Index Terms*— Antenna diversity, antenna gain, antenna pattern synthesis, antenna radiation patterns, antennas, arrays, communication channels, direction of arrival (DoA) estimation.**

I. Introduction

UNMANNED aerial vehicles (UAVs) are one of the most important innovations in the area of aeronautics. Small UAVs are being capable of package delivery, large UAVs operate, for instance, as taxis. Safe integration in the airspace is a major issue in terms of reliability and authorization. Autonomous flight controls can either help pilots in rough environments to start and land safely, while ensuring collision avoidance to other aerial vehicles. Both cooperative as well as noncooperative vehicles need to be targeted. In [1], both cooperative as well as noncooperative sensors are discussed, while focus is on cooperative collision avoidance based on Airborne Collision Avoidance System (ACAS) and Automatic Dependent Surveillance (ADS). The system is based on transponder communication in the 1030/1090 MHz band. However, if the position of the target is not transmitted, commonly a primary radar is used by traffic control to identify the position of the transponder. To make use of as many information as possible by the transponder communication, a direction of arrival (DoA) estimation in conjunction with the transponder communication is of interest.

In [2], different approaches for channel modeling in aerial scenarios are described. A literature survey on channel models, including polarization, is conducted in [3] and [4]. Generally, however, neither special antenna patterns nor exact polarizations are treated. In [5], a geometry-based polarization model is proposed, based on field measurements. A multiple-input multiple-output (MIMO) channel model for UAVs is discussed in [6], where random distributions for the model are determined. However, finally, random distributions are used for the calculation of a cross-polarization matrix.

Commonly, for DoA estimation an antenna array is used, which allows to measure time and phase relationship between the ports of the antenna elements [7]. Most often, just one antenna type is used for all elements. Hence, the antenna radiation patterns of all antenna ports of the array are the same. If linear or square structures are used to form the array, a uniform linear/planar array (ULA/UPA) is created.

In [8], another attractive technique for DoA estimation using electromagnetic vector sensors (EMVS) was introduced. EMVS antennas have the ability to recover the complete information available in an electromagnetic wave by sensing both the electric and magnetic fields. For that purpose, a structure of orthogonal antenna elements is applied [9]. EMVS antennas are designed to allow precise DoA estimation, while, on the other hand, offer communication options.

Another option are multimode antennas. Multimode antennas offer different orthogonal radiation patterns on a single radiator, providing independent antenna ports. They deploy the theory of characteristic modes [10] on a single radiator for designing a compact multiport antenna typically used for digital communications. Multimode antennas have extensively been investigated both for high-speed massive MIMO communications as well as IoT applications with massive connectivity [11]. However, they are also capable of being used for DoA estimation purposes as demonstrated in [12]

Manuscript received 9 August 2021; revised 6 May 2022; accepted 30 June 2022. Date of publication 21 July 2022; date of current version 17 November 2022. This work was supported in part by the German Federal Ministry for Economic Affairs and Climate Action (BMWK) on the basis of a decision by the German Bundestag through the Master360 Program under Research Grant 20D1905I. *(Corresponding author: Nils Lennart Johannsen.)*

The authors are with the Faculty of Engineering, Kiel University, 24143 Kiel, Germany (e-mail: nj@tf.uni-kiel.de; saaa@tf.uni-kiel.de; ph@tf.uni-kiel.de).

Color versions of one or more figures in this article are available at https://doi.org/10.1109/TAP.2022.3191418.

Digital Object Identifier 10.1109/TAP.2022.3191418

and [13] for the planar multimode antenna design proposed in [14].

Overall, both multimode and EMVS antennas are alternatives to conventional antenna arrays from different perspectives. We believe that multimode antennas are an attractive solution for UAV applications because they are useful to reduce weight and surface area. It is likely that a limited number of these antennas is spatially distributed in three dimensions over the surface of the UAV. The resulting array generally cannot be described by a uniform structure. This leads to a more complex modeling of the overall antenna array as shown in [15].

In this article, a novel approach to model the channel for both DoA estimation as well as transponder-based communication between UAVs is proposed. To be able to model arbitrary path geometries, the manifold matrix of the multimode antennas positioned on the UAV is taken into account. Positioning of multimode antennas given an arbitrary UAV size is demonstrated. The patterns and array responses of the individual antenna ports are combined in a matrix representing all ports of the antenna array. Depending on the rotation of the UAV, the response is provided for vertically polarized waves. For visualization, the resulting gain patterns of the antennas are shown. The possibility toward MIMO channel modeling by using manifold matrices is discussed. The manifold matrix is used for an optimization of the radiation characteristic toward omnidirectional radiation in the zero-degree elevation plane and allows DoA estimation as done in [7] and [16]. Different optimization functions are discussed and an additional optimization for vertically polarized waves is conducted.

II. Calculation of the UAV Manifold

In this section, the geometry-based channel modeling approach is described. It is organized by the following subsections. Section II-A, the antenna positioning and orientation is described and the antenna pattern response is determined. Section II-B, the array response based on the different antenna positions is included. Section II-C, the antenna pattern response to the incident type of wave is determined and the antenna response given a desired polarization is calculated.

A. Antenna Positioning and Response

To be able to create an arbitrary channel matrix using a possible arbitrary number of rays and scatterers, a general representation of the antenna and array response of the UAV needs to be calculated. This can be done in terms of a manifold matrix. The manifold matrix for the UAV is a generalization of the well-known array equation but contains arbitrary antenna positions, orientations as well as different antenna patterns, as required for the employed multimode antennas. The manifold matrix $\boldsymbol{M}_{\mathrm{pol}} = f(\boldsymbol{M}_{\phi}, \boldsymbol{M}_{\theta})$ holds the response of each antenna element and mode for all possible incident angles. Each element during the generation of the channel is represented by its position and rotation relative to the next level of elements. As an example, each UAV has a 3-D position in the airspace, which is described by the position vector $\boldsymbol{p}_{\mathrm{UAV}}$. The positions of the antennas of the UAV defining an array are given by the antenna elements position vectors, $\boldsymbol{p}_{\mathrm{Ant},a}$. The initial positions are determined by length l, height h, and width w of the UAV. As a first approximation, a cuboid is used. The position vectors of the antennas on the UAV are stored column-wise in a position matrix $\boldsymbol{P}_{\mathrm{Ant}}$. Given the UAVs center at the origin of a global coordinate system, the initial antenna positions are set to be centered on each axis

$$\boldsymbol{P}_{\mathrm{Ant}} = \begin{bmatrix} -l/2 & l/2 & 0 & 0 & 0 & 0 \\ 0 & 0 & -w/2 & w/2 & 0 & 0 \\ 0 & 0 & 0 & 0 & -h/2 & h/2 \end{bmatrix}. \quad (1)$$

Note that the last two columns are only of interest, if not four but six antennas, also located on the top and at the bottom of the UAV, are employed. For each antenna at the UAV additional to the position the orientation of the antenna is required. The rotation matrix $\boldsymbol{R}_{\mathrm{Ant},a}$ stores the orientation of the antenna element compared to the UAV. Any rotation matrix in the context of this model is defined by, (2), as shown at the bottom of the next page, where φ is the roll angle, ϑ the pitch angle, and ψ the yaw angle, respectively. Furthermore, the orientation of the UAV is stored by means of a rotation matrix $\boldsymbol{R}_{\mathrm{UAV}}$. This rotation matrix is defined as in (2). If a rotation is applied to the UAV, the antenna positions $\boldsymbol{P}'_{\mathrm{Ant}}$ can be calculated by

$$\boldsymbol{P}'_{\mathrm{Ant}} = \boldsymbol{R}_{\mathrm{UAV}} \boldsymbol{P}_{\mathrm{Ant}}. \quad (3)$$

The employed representation of the rotation corresponds to a rotation of the order roll, pitch, and yaw, if the rotation matrix is applied from the left. Hence, the antenna rotation angles are as follows:

$$\boldsymbol{A}_{\varphi,\vartheta,\psi} = \begin{bmatrix} 0 & 0 & \pi/2 & -\pi/2 & \pi & 0 \\ -\pi/2 & \pi/2 & 0 & 0 & 0 & 0 \\ 0 & 0 & 0 & 0 & 0 & 0 \end{bmatrix}. \quad (4)$$

Given an antenna pattern of a planar multimode antenna as proposed in [14], the antenna is designed in the x–y-plane, while the pattern points to the positive z-axis hemisphere. The antennas under assumption are planar antennas based above a ground plane as described in [14] and [17]. These antennas are expected to be mounted on wings and fuselage, which extend the ground plane. Hence, their normal vectors are perpendicular to the structure of the UAV. A small impact of coupling when using an array of multimode antennas is shown in [14]. Additionally, the impact of coupling between the elements is further reduced by the large spacing between the antenna elements on the UAV. Therefore, coupling between the antenna elements has no significant impact on the beamforming behavior.

In Fig. 1, the positions of the antennas on the UAV as well as the norm vectors of the antennas are depicted. To calculate the manifold matrix $\boldsymbol{M}_{\mathrm{pol}}$, an incident planar wavefront from all angles of the full sphere surrounding the UAV is assumed iteratively. Subsequently, and without loss of generality, the UAV is assumed to be located with its center at the origin of the global coordinate system. The incident angles ϕ_{UAV} and θ_{UAV} describe the direction from which the incident wavefront is impinging. Hence, the corresponding unit vector $\boldsymbol{k}_{\mathrm{UAV}}$ from

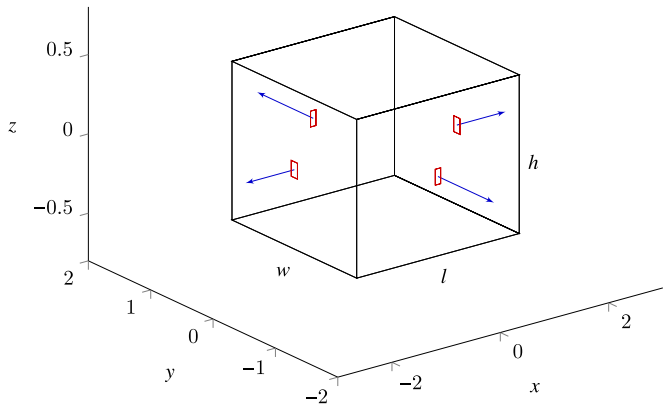

Fig. 1. Antenna positions on the UAV.

the UAV toward the wavefront $\boldsymbol{k}_{\text{inc}}$ is described by

$$-\frac{\lambda}{2\pi}\boldsymbol{k}_{\text{inc}} = \boldsymbol{k}_{\text{UAV}} = \begin{bmatrix} \cos\phi_{\text{UAV}} \sin\theta_{\text{UAV}} \\ \sin\phi_{\text{UAV}} \sin\theta_{\text{UAV}} \\ \cos\theta_{\text{UAV}} \end{bmatrix}. \tag{5}$$

The factor $(\lambda/2\pi)$ normalizes the wave vector $\boldsymbol{k}_{\text{inc}}$ to unit length, where λ is the wavelength. Let

$$\underline{\boldsymbol{E}}(\phi_{\text{Ant}}, \theta_{\text{Ant}}) = \begin{bmatrix} \underline{E}_{\phi,m}(\phi_{\text{Ant}}, \theta_{\text{Ant}}) \\ \underline{E}_{\theta,m}(\phi_{\text{Ant}}, \theta_{\text{Ant}}) \end{bmatrix} = F_m(\phi_{\text{Ant}}, \theta_{\text{Ant}}) \tag{6}$$

$$\frac{1}{2Z_{\text{F}}} \oint_{\Omega} |\underline{\boldsymbol{E}}(\phi_{\text{Ant}}, \theta_{\text{Ant}})|^2 d\Omega = 1 \tag{7}$$

denote a function which gets the complex electric field components of the antenna response vector $\underline{E}_{\phi}$ and $\underline{E}_{\theta}$. The surface integral defines the power normalization, with $Z_{\text{F}} = 120\pi\ \Omega$ being the field resistance. When the integral in (7) is solved for a unit-sphere, a factor of $(4\pi/2Z_{\text{F}})$ remains. Hence, the field components of an isotropic radiator have amplitudes of $\sqrt{60}$. The angles ϕ_{Ant} and θ_{Ant} define the direction of a wave impinging on the antenna. The index m represents the mth port of the multimode antenna. For the calculation of the antenna incident angles, the rotation matrix of the antenna element and, if required, of the UAV needs to be applied. The rotation of the antenna can be described by an inverted rotation of the UAVs wave vector

$$\boldsymbol{k}_{\text{Ant}} = \boldsymbol{R}_{\text{UAV}}^{T} \boldsymbol{R}_{\text{Ant}}^{T} \boldsymbol{k}_{\text{UAV}}. \tag{8}$$

The inversion is achieved by using the transpose of the rotation matrices, since they are orthogonal. The corresponding incident angles can then be calculated by the standard calculations

$$\phi_{\text{Ant}} = \text{arctan2}\{\boldsymbol{k}_{\text{Ant},2}, \boldsymbol{k}_{\text{Ant},1}\} \tag{9}$$

$$\theta_{\text{Ant}} = \arccos\{\boldsymbol{k}_{\text{Ant},3}\} \tag{10}$$

where $\boldsymbol{k}_{\text{Ant},i}$ is the ith component of the vector, and $\text{arctan2}\{y, x\}$ denotes the two-argument arctangent to calculate the correct quadrant in the Euclidean plane.

B. Array Response

For the calculation of the phase of the array response of the UAV, the well-known array equation

$$\bar{\gamma}_{\text{Ant}} = \frac{2\pi}{\lambda} \boldsymbol{k}_{\text{UAV}} \cdot \boldsymbol{p}_{\text{Ant}} \tag{11}$$

is applied. The phase angle γ is calculated for each antenna position $\boldsymbol{p}_{\text{Ant},a}$ given by the positions in $\boldsymbol{P}_{\text{Ant}}$. Depending on calculating the manifold matrix for a transmit or receive scenario, the phase γ is applied with either negative or positive sign according to

$$\gamma_{\text{Ant}} = \begin{cases} \bar{\gamma}_{\text{Ant}}, & \text{if Tx} \\ -\bar{\gamma}_{\text{Ant}}, & \text{if Rx.} \end{cases} \tag{12}$$

Finally, the phase needs to be applied to the corresponding antenna element.

C. Polarization Calculation

If an antenna is assumed to be located without rotation, the θ-component corresponds to a vertically polarized wave and the ϕ-component to the horizontally polarized wave. Since the UAV employs an arbitrary number of antennas (we assume four antennas), which are pointing to different directions, the assumption of the polarization does not hold anymore. In typical wireless channel models (e.g., [4]), the impact of polarization is not treated at all (Rayleigh channels, geometry-based stochastic models [6]), or by the introduction of a cross-polarization matrix, as in [3] and [18]. There, the cross polarization coefficients are defined by stochastic processes given a certain type and variance. Regarding stochastic channel models with non-line-of-sight (NLOS), polarization misalignment and its consequences are rather of interest in terms of average channel performance and Monte Carlo simulations are used. However, in the context of the described airborne scenario, DoA estimation shall be performed. Since in aerial applications line-of-sight (LOS) communication is likely in most cases, the impact of its polarization is expected to contribute mainly to the receive signal of the UAV. Having the global incident angles ϕ_{UAV} and θ_{UAV} defined, the vertical and horizontal field components are represented by the unit sphere vectors $\boldsymbol{e}_{\phi,\text{inc}}$ and $\boldsymbol{e}_{\theta,\text{inc}}$. The corresponding vectors in Cartesian coordinates can be determined by applying the transformation matrix

$$\boldsymbol{S}(\phi, \theta) = \begin{bmatrix} \sin\theta\cos\phi & \cos\theta\cos\phi & -\sin\phi \\ \sin\theta\sin\phi & \cos\theta\sin\phi & \cos\phi \\ \cos\theta & -\sin\theta & 0 \end{bmatrix}. \tag{13}$$

Hence, the unit Cartesian vectors of the vertical and horizontal incident wave are defined by

$$\boldsymbol{e}_{\text{v}} = \boldsymbol{S}(\phi_{\text{inc}}, \theta_{\text{inc}})\ \boldsymbol{e}_{\theta,\text{inc}} \tag{14}$$

$$\boldsymbol{e}_{\text{h}} = \boldsymbol{S}(\phi_{\text{inc}}, \theta_{\text{inc}})\ \boldsymbol{e}_{\phi,\text{inc}}. \tag{15}$$

$$\boldsymbol{R}(\varphi, \vartheta, \psi) = \begin{bmatrix} \cos(\psi)\cos(\vartheta) & \cos(\psi)\sin(\vartheta)\sin(\varphi) - \sin(\psi)\cos(\varphi) & \cos(\psi)\sin(\vartheta)\cos(\varphi) + \sin(\psi)\sin(\varphi) \\ \sin(\psi)\cos(\vartheta) & \sin(\psi)\sin(\vartheta)\sin(\varphi) + \cos(\psi)\cos(\varphi) & \sin(\psi)\sin(\vartheta)\cos(\varphi) - \cos(\psi)\sin(\varphi) \\ -\sin(\vartheta) & \cos(\vartheta)\sin(\varphi) & \cos(\vartheta)\cos(\varphi) \end{bmatrix} \tag{2}$$

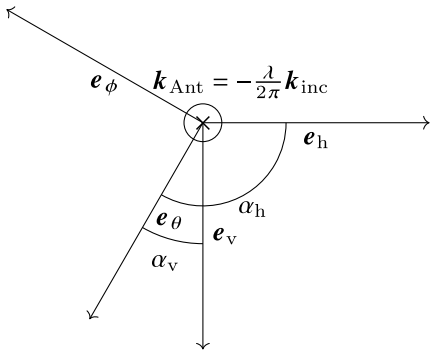

Fig. 2. Field components in the projection plane for the definition of α.

The vertically and horizontally polarized unit Cartesian vectors can be used to describe a projection plane. The unit Cartesian vectors of each antenna have to be projected to this plane. Then, the resulting polarization angle can be calculated. Note that the angles of the incident wave are used, rather than the incident angles of the UAV. As a result, when aligned perfectly, the vertical unit vectors of both, antenna and incident wave point in the same direction, while the horizontal components point in opposite directions. This is due to the opposite direction of the wave vectors of the antenna and incident wave. Fig. 2 shows a general misaligned case. The angles ϕ_{Ant} and θ_{Ant} from (9) and (10) can be used as in (13)–(15) to calculate the projection of the unit Cartesian vectors of the antenna

$$\boldsymbol{e}_\theta = \boldsymbol{S}(\phi_{\mathrm{Ant}}, \theta_{\mathrm{Ant}})\ \boldsymbol{e}_{\theta,\mathrm{inc}} \tag{16}$$

$$\boldsymbol{e}_\phi = \boldsymbol{S}(\phi_{\mathrm{Ant}}, \theta_{\mathrm{Ant}})\ \boldsymbol{e}_{\phi,\mathrm{inc}}. \tag{17}$$

The polarization angle α is defined as depicted in Fig. 2. It is calculated by using the two scalar products

$$\alpha_{\mathrm{v}} = \arccos \frac{\boldsymbol{e}_\theta^T \boldsymbol{e}_{\mathrm{v}}}{|\boldsymbol{e}_\theta| \cdot |\boldsymbol{e}_{\mathrm{v}}|} \tag{18}$$

$$\alpha_{\mathrm{h}} = \arccos \frac{\boldsymbol{e}_\theta^T \boldsymbol{e}_{\mathrm{h}}}{|\boldsymbol{e}_\theta| \cdot |\boldsymbol{e}_{\mathrm{h}}|}. \tag{19}$$

A distinction of cases sets the value of α as

$$\alpha = \begin{cases} \alpha_{\mathrm{v}}, & \text{if } \alpha_{\mathrm{h}} \geq \pi/2 \\ 2\pi - \alpha_{\mathrm{v}}, & \text{else.} \end{cases} \tag{20}$$

Given the electric field components of the antenna pattern by (6), the vertical and horizontal field components can be calculated by applying

$$\begin{bmatrix} \underline{E}_{\mathrm{v},m} \\ \underline{E}_{\mathrm{h},m} \end{bmatrix} = \begin{bmatrix} -\sin\alpha & \cos\alpha \\ -\cos\alpha & -\sin\alpha \end{bmatrix} \begin{bmatrix} \underline{E}_{\phi,m} \\ \underline{E}_{\theta,m} \end{bmatrix}. \tag{21}$$

The manifold matrix, e.g., for vertical polarization can be calculated by merging the intermediate results to

$$M_{a,m,\mathrm{v}}(\phi,\theta) = \underline{E}_{\mathrm{v},m}(\phi,\theta)\ e^{j\gamma(\phi,\theta)} \tag{22}$$

where $M_{a,m,\mathrm{v}}(\phi,\theta)$ is the element ϕ,θ of the vertical polarization manifold matrix of the mth port and ath antenna.

D. Application Example

Under the assumption of a typical airborne transponder scenario, the simplest case is a single-input multiple-output (SIMO) scenario. Hence, the creation of a SIMO model is described subsequently, but the same steps can be used to model an MIMO scenario. Let us assume that one vertically polarized wave is transmitted from a ground-based air surveillance system or an interrogator positioned in any other aerial vehicle, which requests the transponder to answer. Given a high antenna directivity at the air surveillance system and a sufficient flight altitude, no severe scattering has to be expected. Since transponder signals are narrowband and vertically polarized, a simple model consists of the manifold matrix for the vertical polarized wave of the receive antenna $\boldsymbol{m}_{\mathrm{v,R}}$, and a correction term including attenuation and normalization according to

$$\boldsymbol{h}_{\mathrm{LOS,SIMO}} = \frac{L}{\sqrt{60}} \boldsymbol{m}_{\mathrm{v,R}}\, e^{j\Upsilon}. \tag{23}$$

The path attenuation is represented by L, the normalization factor of $\sqrt{60}$ is due to the comparison to isotropic radiation from (7). The vector $\boldsymbol{m}_{\mathrm{v}}$ represents the manifold vector for all ports in LOS direction and Υ the phase of the transmission link. For other polarizations, arbitrary combinations of the two manifold matrices for vertical and horizontal polarizations can be employed. If additional propagation paths shall be added, a cross correlation matrix can be used which represents the change of polarization due to the impact of scatterers. Then, the scattering characteristics can be described as for common channel models as in [18]. If an MIMO system shall be employed (e.g., consisting of two UAVs), the manifold matrix for both UAVs needs to be calculated as discussed in (22). The choice of the incident angles at both UAVs determines the relative position between them. Once a LOS connection is defined, arbitrary additional paths can be defined as in [5].

In Fig. 3, the antenna gain patterns mounted at the UAV in the global x-y-plane are depicted. For this model, the multimode antenna proposed in [14] is employed. As can be seen, the patterns of the left/right and front/rear antenna are different, although the same antenna is used. This is due to the different orientations. This can be explained by the fact that for the antennas at the front and back a cut in the x–z-plane of the antenna is performed, while for the antennas at the left and right the rotation results in a cut in the y–z-plane of the antennas. As an example, the initially backward pointing side of the antenna element is pointing upward for the front antenna while it is pointing downward for the antenna placed at the back of the UAV.

III. Radiation Optimization

In classical airborne scenarios, the interrogators use quarter-wavelength stub-antennas for their transmissions [19]. However, when the implementation of additional DoA estimation is desired, these stub-antennas are not sufficient. As shown in [12], multimode antennas can be used for this task. Opposed to the stub-antennas, multimode antennas do not provide an omnidirectional radiation behavior. If several multimode

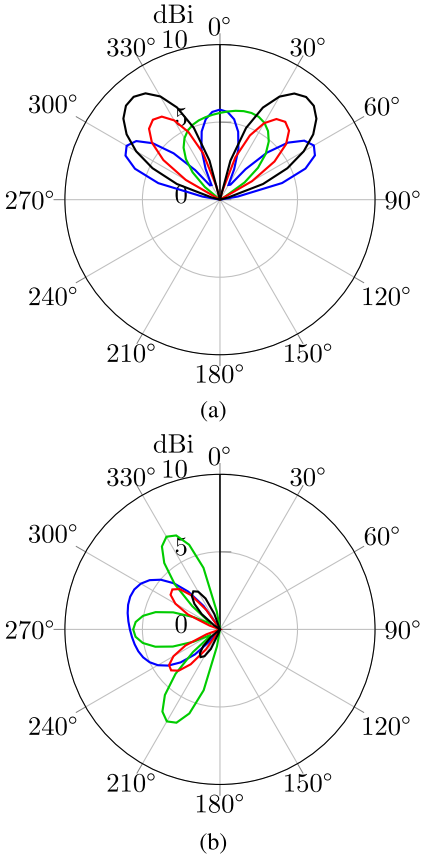

Fig. 3. Gain patterns of the antennas. Note that the patterns depend on the rotation of the individual antenna. The data needed for a reconstruction of the patterns are provided in [13]. (a) Front/rear antenna. (b) Left/right antenna.

antennas are located at the different sides of the UAV as discussed in Section II, an omnidirectional radiation is even more difficult to achieve due to the array characteristics resulting from the positions of the antennas. Subsequently, the manifold matrices calculated in Section II are used to optimize the overall radiation based on digital beamforming, which allows arbitrary amplitudes and phases at each port. A pattern-based beamforming for multimode antennas is described in [20], where a maximization of the gain toward a certain angle is targeted.

A. Problem Formulation

In a first approach, the omnidirectional behavior of the antenna array located on the UAV is targeted. Next, an additional maximization of gain is of interest. Finally, to improve the capabilities for transmissions using interrogators, the vertically polarized radiated power is maximized. As described in [15], the antenna-and-array factor (AAF) can be calculated by

$$\mathrm{AAF}(\phi,\theta)=\frac{4\pi}{2Z_\mathrm{F}}\left[\left|\sum_a\sum_m M_{a,m,\mathrm{v}}(\phi,\theta)\,c_{a,m}\right|^2+\left|\sum_a\sum_m M_{a,m,\mathrm{h}}(\phi,\theta)\,c_{a,m}\right|^2\right] \tag{24}$$

which is a generalization of the well-known array equation to fit multimode antennas. Unlike classic precoding techniques, when using multimode antennas, the pattern of the antenna ports have to be taken into account instead of restricting the optimization to the array factor. For isotropic radiation, the minimum and the maximum of the AAF

$$\mathrm{AAF}_\mathrm{min}=\min_{\phi,\theta}\ \{\mathrm{AAF}(\phi,\theta)\} \tag{25}$$

$$\mathrm{AAF}_\mathrm{max}=\max_{\phi,\theta}\ \{\mathrm{AAF}(\phi,\theta)\} \tag{26}$$

should ideally be the same. Therefore, a simple objective function is

$$\min_{\boldsymbol{c}}\ \left\{\frac{\mathrm{AAF}_\mathrm{max}-\mathrm{AAF}_\mathrm{min}}{\mathrm{AAF}_\mathrm{max}}\right\},\quad \text{s.t. } |\boldsymbol{c}|^2\le 1. \tag{27}$$

The objective function from (27) can be generalized as

$$\mathrm{Obj1}:=\min_{\boldsymbol{c}}\ \left\{\frac{(\mathrm{AAF}_\mathrm{max}-\mathrm{AAF}_\mathrm{min})^a}{\mathrm{AAF}_\mathrm{max}^b}\right\}. \tag{28}$$

The exponents a and b can be used to control the impact of either difference or maximum AAF, respectively. However, throughout the simulations conducted in this article, a and b are set to be one. A disadvantage of using this objective is the fact that similar results are achieved when either both values are small (which is not desired) or both values are large (which is desired). As an example, for very small radiated powers, the fraction might become small as well. A different approach to solve this issue is using logarithmic functions

$$\mathrm{Obj2}:=\min_{\boldsymbol{c}}\ \left\{\log_{10}(\mathrm{AAF}_\mathrm{max})-2\log_{10}(\mathrm{AAF}_\mathrm{min})\right\}. \tag{29}$$

Using the objective function Obj2 tends to select larger gains compared to Obj1. For both, simulation results are given in Section III-D.

B. Particle Swarm Optimization Using Norm Ball

Since the input power is defined by the norm of the weighting vector $P_\mathrm{T}=|\boldsymbol{c}|^2=1$, the positions of the particles can be described using spherical coordinates in $(2\,N_\mathrm{p})$-dimension. N_p denotes the total number of ports in the antenna array. This allows the reduction of the problem by two dimensions: from the fact of the constant input power, the radius can be set to be one and one coefficient can be defined to be real-valued. This simplification can be proven as follows. Let $\boldsymbol{c}_\mathrm{b}$ be any best solution to fit the isotropic radiation target. Then, the AAF at any point is calculated according to (24) by

$$\mathrm{AAF}_\mathrm{b}(\phi,\theta)=\frac{4\pi}{2Z_\mathrm{F}}\left[\left|\sum_{p=1}^{N_\mathrm{P}} M_{p,\mathrm{v}}(\phi,\theta)\,c_{p,\mathrm{b}}\right|^2+\left|\sum_{p=1}^{N_\mathrm{P}} M_{p,\mathrm{h}}(\phi,\theta)\,c_{p,\mathrm{b}}\right|^2\right]. \tag{30}$$

The index p of the sum corresponds to the port of the array. If the first element of the sum is separated and the

sum is extended by the negative phase of the first weighting coefficient φ_1, (30) can be rewritten as

$$\mathrm{AAF_b} = \frac{4\pi}{2Z_\mathrm{F}}\left[\left|M_{1,\mathrm{v}}\,|c_{1,\mathrm{b}}| + \sum_{p=2}^{N_\mathrm{P}} M_{p,\mathrm{v}}\,c_{p,\mathrm{b}}\,\mathrm{e}^{-j\varphi_1}\right|^2 + \left|M_{1,\mathrm{h}}\,|c_{1,\mathrm{b}}| + \sum_{p=2}^{N_\mathrm{P}} M_{p,\mathrm{h}}\,c_{p,\mathrm{b}}\,\mathrm{e}^{-j\varphi_1}\right|^2\right] \quad (31)$$

where the argument (ϕ, θ) is omitted for the reason of simplicity. By applying the phase of the first coefficients to the others, any solution becomes unique and the solution space is reduced by another dimension. In particle swarm optimization (PSO), spherical coordinates of dimension $2\,N_\mathrm{P} - 1$ can be used to implement this reduction. These contain $2\,N_\mathrm{P} - 2$ angles and the radius. For a description the PSO algorithm, the reader is referred to [21]–[23]. As mentioned above, the radius is set to be 1 by definition. The positions of the particles, which refer to the chosen set of coefficients $\boldsymbol{c}$ can be calculated by

$$\begin{aligned}
\Re\{c_1\} &= \cos\varphi_1 \\
\Re\{c_2\} &= \sin\varphi_1 \cos\varphi_2 \\
\Im\{c_2\} &= \sin\varphi_1 \sin\varphi_2 \cos\varphi_3 \\
&\vdots \\
\Re\{c_{N_\mathrm{P}}\} &= \left(\prod_{n=1}^{2N_\mathrm{P}-3} \sin\varphi_n\right)\cos\varphi_{2N_\mathrm{P}-2} \\
\Im\{c_{N_\mathrm{P}}\} &= \prod_{n=1}^{2N_\mathrm{P}-2} \sin\varphi_n
\end{aligned} \quad (32)$$

where $\Re\{.\}$ and $\Im\{.\}$ denote the real and imaginary parts of the argument.

C. Optimization of Vertically Polarized Power

As discussed in Section I, for aerial applications vertically polarized signals are used. Typically, a quarter-wavelength stub antenna is employed at the top and bottom of an aircraft [19]. Multimode antennas employ several modes and therefore not only vertically polarized antenna patterns. To improve the properties of the transmission channel, an optimization of the vertically polarized power while maintaining an omnidirectional behavior is discussed. To achieve this goal, (29) is modified as

$$\mathrm{Obj2_v} := \min_{\boldsymbol{c}} \Big\{\log_{10}(\mathrm{AAF_{max}}) - \log_{10}(\mathrm{AAF_{min}}) - \log_{10}(\mathrm{AAF_v})\Big\}. \quad (33)$$

The power of the vertical field component is represented by $\mathrm{AAF_v}$, where only the portion regarding the vertical field components in (24) is taken into account.

D. Numerical Results

In this section, the results using different objective functions are discussed. Further on, the results of different strategies of optimizing the overall radiation characteristic are provided.

TABLE I
COMPARISON OF THE OBJECTIVE FUNCTIONS

Optimization Function	Average fitness (50 Runs) tested by Obj1	Obj2
Obj1	0.29	-1.93
Obj2	0.33	-2.09

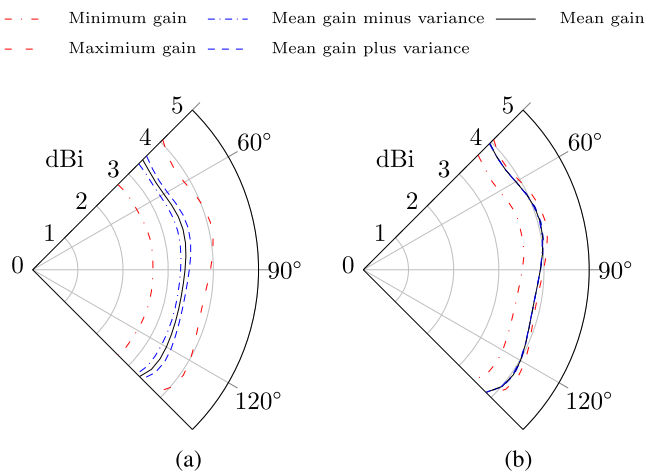

Fig. 4. Radiation optimization for the right antenna between the angles of 45° and 135°. The 5% providing the worst values are neglected during the optimization. The graphs show the average performance based on 50 runs. It can be seen that (29) provides a more stable performance and higher gain than (28) on average. (a) Optimization using (28). (b) Optimization using (29).

1) Comparison of Objective Functions: As can be seen in Fig. 4, both objective functions provide a more or less omnidirectional radiation when applied for an interval of a single antenna. The optimization is performed for the right antenna in the region of 45°–135°, which corresponds to the region toward which the right antenna is pointing. For each optimization, 50 runs have been performed and the corresponding mean pattern and variances are plotted. The 5% of angles having the worst performance are neglected, which allows better focus on the achievable gain. The objective function Obj1 provides a flat characteristic, while Obj2 provides a larger gain as well as more stable performance. Another possibility to compare the performance of an objective function under test is a cross-check: the resulting precoding vectors of the first objective function are applied to the second objective function and vice versa. A comparison is provided in Table I. As can be found, both objective functions achieve good results calculating fitness values of the other objective function. However, objective function Obj2 tends to first achieve more stable results as well as achieving the higher gain, which is of interest in communication systems. Therefore, it is chosen for the optimization of the full plane. As can be seen in Fig. 5, the achieved gain pattern provides a gain between -1 and 2 dBi for almost all angles and realizations. Accordingly, more or less all points are inside the 3 dB beamwidth. The gain pattern could be flattened by either using Obj1 instead of Obj2 at the cost of directivity. Compared to the radiation pattern in Fig. 4(b), the achieved gain is reduced. This is due to the normalization of the input

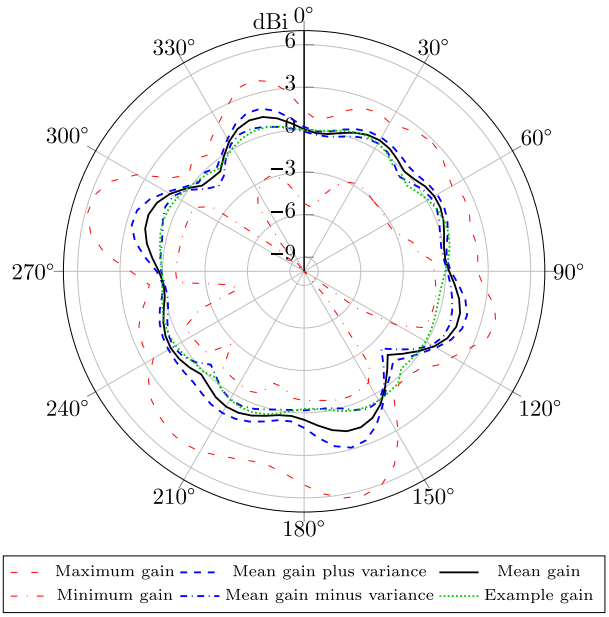

Fig. 5. Optimization of the radiation of the full sphere employing the full antenna array using (29). The lines represent the average result of the optimization, using 50 runs. Minimal gain, maximal gain (red curves), as well as mean gain (black curve), and the mean gain plus/minus the variance (blue curves) are shown as well as an example plot of an achievable pattern (green curve).

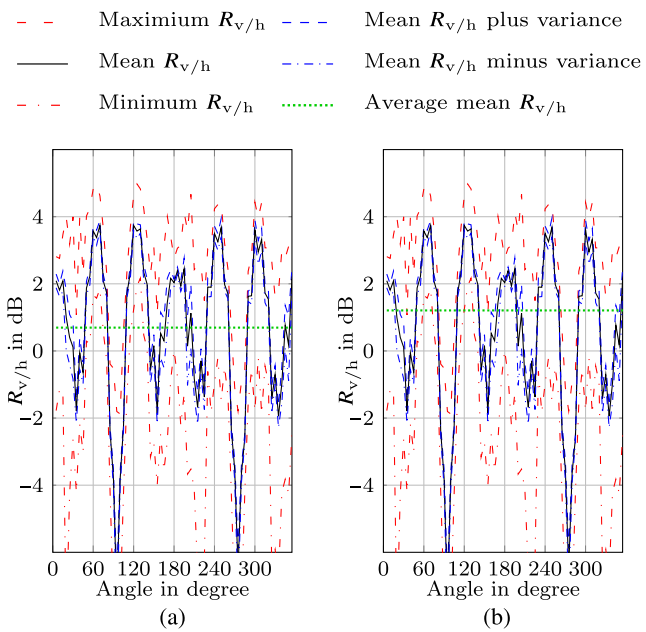

Fig. 6. Comparison of the power ratio $R_{v/h}$ from (34) for vertically and horizontally polarized power is shown, using the objective functions Obj2 and Obj2$_v$. The latter provides better power allocation in terms of vertically polarized power. This can be seen from the achieved average mean of the power ratio $R_{v/h}$. (a) Optimized using Obj2. (b) Optimized using Obj2$_v$.

power provided by the constraint in (27), which of course applies to a single antenna in the same way as for the full antenna array.

2) Optimization of the Vertically Polarized Component: For the comparison of the different patterns in terms of vertically radiated power, the ratio of the power $R_{v/h}$ contributed by the vertical and horizontal field component is calculated by

$$R_{v/h} = 10 \log_{10} \frac{\mathrm{AAF_v}}{\mathrm{AAF_h}} \tag{34}$$

where $\mathrm{AAF_v}$ and $\mathrm{AAF_h}$ denote the AAF calculated for either field component only. As can be seen for Obj2 in Fig. 6(a), the mean of the power ratio $R_{v/h}$ is lower than for the modified version Obj2$_v$ in Fig. 6(b). The corresponding patterns of the AAFs are provided in Fig. 7. As can be seen, the pattern can rarely be regarded as omnidirectional, since the fluctuation of the gain as a function of the angle is much higher compared to Fig. 5. However, for most of the angles, a gain of at least -2 dBi is achieved, which avoids blindness for most angles. From this weaker performance, it is concluded that a different design of the multimode antenna allowing vertically polarized waves is of interest.

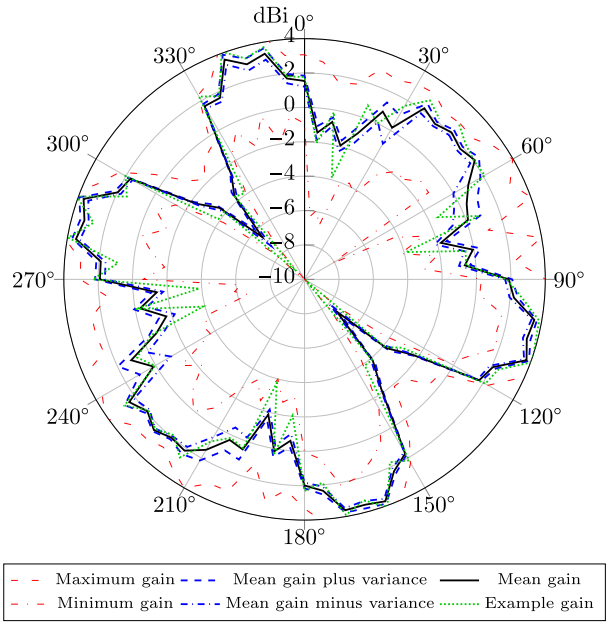

Fig. 7. Optimization of the radiation of the full sphere employing the full antenna array using (33). The optimization of the portion of vertically polarized fields jeopardizes the overall performance. The lines represent mean, variance, minimum, and maximum values of the average result, as well as an arbitrary example curve, using 50 runs.

IV. Realization of Omnidirectional Beamforming

In this section, a metrological verification of the proposed possibilities of the multimode antennas using the optimization approach given the proposed manifold calculation is provided.

A. Antenna Under Consideration

The antenna under consideration is a six-port ultrawideband planar patch antenna as described in [17]. The antenna consists of a planar, square-shaped radiator, arranged in parallel above a square-shaped ground plane. The ground plane is used to provide the feeding network of the radiator. Due to hardware limitations, only four ports can be exploited. For this reason, four out of six ports need to be selected. Toward this goal, the following procedure is proposed: first, the PSO algorithm introduced in Section III-B is run 50 times for all six ports

TABLE II

AVERAGE POWER $|c_p|^2$ SCHEDULED DURING THE OPTIMIZATION USING 50 RUNS. NOTE THAT THE SUM OF THE AVERAGE POWERS DOES NOT HAVE TO BE EQUAL TO ONE

Port 1	Port 2	Port 3	Port 4	Port 5	Port 6
0.0133	0.0683	0.0226	0.2760	0.4559	0.1012

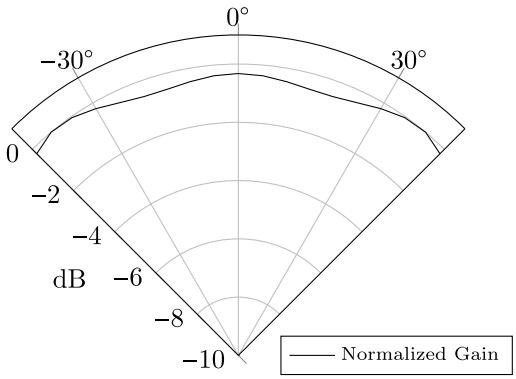

Fig. 8. Optimization result using the ports 2, 4–6 of the antenna. The pattern is normalized to maximum gain. The precoding coefficients are [0.23; $-0.60 - j0.02$; 0.77; 0]. As can be seen, the sixth port is not used and the precoding coefficients are mainly real-valued.

in order to perform a proper power allocation. The average transmit power per port is listed in Table II.

Second, the two ports with the smallest transmit power are removed from the set (here: port numbers 1 and 3). Finally, the PSO algorithm is run again for the remaining four ports 2, 4–6. In this special case, the transmit power at port 6 turns out to be zero. Hence, only three ports are required to achieve a nearly omnidirectional pattern. Still, the resulting performance using the entries of the codebook promises good results, as seen in Fig. 8.

B. Measurement Setup

For the realization, an Ettus USRP N310 software defined radio (SDR) is used to realize the beamforming precoding based on the precalculated codebook entries. The overall system setup and calibration procedure is taken and modified from [24]. The measurement is done using an antenna measurement chamber at Leibniz University Hannover. To achieve phase-coherency, a signal generator provides a 4 GHz sine wave to the local oscillator (LO) inputs of the SDR. The resulting intermediate frequency is 2 GHz. Toward phase calibration, an initial run is started and the differential phase and power of the outgoing wave quantities (b_2/b_1) are measured using a Rohde & Schwarz ZVA 40 Vector Network Analyzer. A stage of mixers is applied to shift the signals to the transmission band at 7.25 GHz. The same calibration procedure was applied to measure the differential phases and gains of the mixers and connected coaxial cables. The output signal of the mixers is taken as input signal for the feeding network of the antenna. The phases of the feeding network of the antenna are known from the antenna design and simulation. The antenna is mounted on a turntable plate, which is rotated during operation. The antenna under investigation is used as a transmitter. At the receiver-side, a horn-antenna, and spectrum analyzer are used for the measurement of either vertical or horizontal polarization. Two measurements are conducted and the received powers are added according to (24). Both, rotation of the antenna and saving of the measurements results are controlled by a computer running MATLAB.

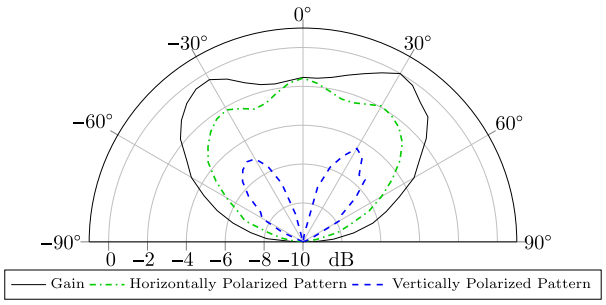

Fig. 9. Normalized plots of the measured gain patterns of the planar antenna. As mentioned in the previous section, a major portion of the radiated fields is polarized horizontally. The measurement is performed at 7.25 GHz, employing the coefficients mentioned in Fig. 8.

C. Measurement Results

In Fig. 9, the resulting gain pattern employing the coefficients calculated for the virtual antenna model are employed. As can be seen, the resulting gain pattern is similar to the one given in Fig. 8.

V. CONCLUSION

In this article, a novel approach toward a simply-applicable physics-based and geometry-based MIMO channel model is presented. This channel model is employable to multimode antennas, but also to classical antennas arrays. The channel model fulfills the requirements for both MIMO communication as well as DoA estimation. The antennas can be placed on arbitrary surface positions on a UAV. Random flight attitudes and their consequences for a given polarization of incident waves are included. The proposed manifold matrix can be used to calculate arbitrary LOS/NLOS paths between a UAV and any other manifold representation. Furthermore, the manifold matrix has been used for the optimization of an omnidirectional radiation characteristic employing a distributed antenna array of four multimode antennas. It is found that good performance is possible, allowing the implementation of multimode antennas for omnidirectional radiation in addition to reception and DoA estimation. However, when vertically polarized waves are of interest, the optimization of the radiation does not provide sufficient performance. The simulation results regarding both the omnidirectional beamforming performance as well as the weak radiation of vertically polarized fields have been proven experimentally. Hence, for the proposed application, conclusions on the design of multimode antenna patterns can be drawn.

ACKNOWLEDGMENT

The cooperative work with Funke GmbH, Heiligenhaus, Germany, and Leibniz University Hannover, Hanover,

Germany, is highly appreciated. The authors would like to express their special thanks to Lukas Grundmann and Dirk Manteuffel at Leibniz University Hannover for their assistance in providing and measuring the antenna.

REFERENCES

[1] G. Manfredi and Y. Jestin, "An introduction to ACAS xu and the challenges ahead," in *Proc. IEEE/AIAA 35th Digit. Avionics Syst. Conf. (DASC)*, Sep. 2016, pp. 1–9.

[2] C. Yan, L. Fu, J. Zhang, and J. Wang, "A comprehensive survey on UAV communication channel modeling," *IEEE Access*, vol. 7, pp. 107769–107792, 2019.

[3] K. Jeon, X. Su, B. Hui, and K. Chang, "Practical and simple wireless channel models for use in multipolarized antenna systems," *Int. J. Antennas Propag.*, vol. 2014, pp. 1–10, Mar. 2014.

[4] K. Zheng, S. Ou, and X. Yin, "Massive MIMO channel models: A survey," *Int. J. Antennas Propag.*, vol. 2014, pp. 1–10, Apr. 2014.

[5] S. Jaeckel, K. Borner, L. Thiele, and V. Jungnickel, "A geometric polarization rotation model for the 3-D spatial channel model," *IEEE Trans. Antennas Propag.*, vol. 60, no. 12, pp. 5966–5977, Dec. 2012.

[6] H. Jiang, Z. Zhang, L. Wu, and J. Dang, "Three-dimensional geometry-based UAV-MIMO channel modeling for A2G communication environments," *IEEE Commun. Lett.*, vol. 22, no. 7, pp. 1438–1441, Jul. 2018.

[7] T. E. Tuncer and F. Friedlander, *Classical and Modern Direction-of-Arrival Estimation*. New York, NY, USA: Academic, 2009.

[8] A. Nehorai and E. Paldi, "Vector-sensor array processing for electromagnetic source localization," *IEEE Trans. Signal Process.*, vol. 42, no. 2, pp. 376–398, Feb. 1994.

[9] J. Duplouy, C. Morlaas, H. Aubert, P. Potier, P. Pouliguen, and C. Djoma, "Wideband and reconfigurable vector antenna using radiation pattern diversity for 3-D direction-of-arrival estimation," *IEEE Trans. Antennas Propag.*, vol. 67, no. 6, pp. 3586–3596, Jun. 2019.

[10] R. Martens and D. Manteuffel, "Systematic design method of a mobile multiple antenna system using the theory of characteristic modes," *Microw. Antennas Propag.*, vol. 8, no. 12, pp. 887–893, Sep. 2014.

[11] N. L. Johannsen, N. Peitzmeier, P. A. Hoeher, and D. Manteuffel, "On the feasibility of multi-mode antennas in UWB and IoT applications below 10 GHz," *IEEE Commun. Mag.*, vol. 58, no. 3, pp. 69–75, Mar. 2020.

[12] R. Pohlmann, S. A. Almasri, S. Zhang, T. Jost, A. Dammann, and P. A. Hoeher, "On the potential of multi-mode antennas for direction-of-arrival estimation," *IEEE Trans. Antennas Propag.*, vol. 67, no. 5, pp. 3374–3386, May 2019.

[13] S. Alkubti Almasri, R. Pohlmann, N. Doose, P. A. Hoeher, and A. Dammann, "Modeling aspects of planar multi-mode antennas for direction-of-arrival estimation," *IEEE Sensors J.*, vol. 19, no. 12, pp. 4585–4597, Jun. 2019.

[14] D. Manteuffel and R. Martens, "Compact multimode multielement antenna for indoor UWB massive MIMO," *IEEE Trans. Antennas Propag.*, vol. 64, no. 7, pp. 2689–2697, Jul. 2016.

[15] N. Doose and P. A. Hoeher, "Joint precoding and power control for EIRP-limited MIMO systems," *IEEE Trans. Wireless Commun.*, vol. 17, no. 3, pp. 1727–1737, Mar. 2018.

[16] Z. Chen, G. Gokeda, and Y. Yu, *Introduction to Direction-of-Arrival Estimation* (Artech House Signal Processing Library). Norwood, MA, USA: Artech House, 2010. [Online]. Available: https://books.google.fr/books?id=_63d0OKsDsAC

[17] N. Peitzmeier and D. Manteuffel, "Upper bounds and design guidelines for realizing uncorrelated ports on multimode antennas based on symmetry analysis of characteristic modes," *IEEE Trans. Antennas Propag.*, vol. 67, no. 6, pp. 3902–3914, Jun. 2019.

[18] P. Kyösti *et al.*, "WINNER II channel models," Inf. Soc. Technol. (IST), Tech. Rep. IST-4-027756 WINNER II D1.1.2 V1.2, 2008. [Online]. Available: http://www.ero.dk/93F2FC5C-0C4B-4E44-8931-00A5B05A331B

[19] The European Organisation for Civil Aciation Equipment, *Minimum Operational Performance Specification for Secondary Surveillance Radar Mode S Transponders*, document ED-73C, May 2008.

[20] N. L. Johannsen and P. A. Hoeher, "Single-element beamforming using multi-mode antenna patterns," , vol. 9, no. 7, pp. 1120–1123, 2020.

[21] R. Eberhart and J. Kennedy, "A new optimizer using particle swarm theory," in *Proc. 6th Int. Symp. Micro Mach. Hum. Sci. (MHS)*, 1995, pp. 39–43.

[22] J. Kennedy and R. Eberhart, "Particle swarm optimization," in *Proc. Int. Conf. Neural Netw. (ICNN)*, vol. 4, 1995, pp. 1942–1948.

[23] Y. Shi and R. Eberhart, "A modified particle swarm optimizer," in *Proc. IEEE Int. Conf. Evol. Comput. IEEE World Congr. Comput. Intell.*, May 1998, pp. 69–73.

[24] D. Marinho, R. Arruela, T. Varum, and J. N. Matos, "Application of digital beamforming to software defined radio 5G/radar systems," in *IEEE MTT-S Int. Microw. Symp. Dig.*, Nov. 2019, pp. 1–3.

Nils Lennart Johannsen received the B.Eng. degree from the Hamburg University of Applied Sciences, Hamburg, Germany, in 2016, and the M.Sc. degree in electrical engineering and information technology from Kiel University, Kiel, Germany, in 2018, where he is currently pursuing the Ph.D. degree with the Chair of Information and Coding Theory, as a Research and Teaching Assistant.

His research interests include massive multiple-input multiple-output (MIMO) systems and baseband signal processing for multimode antennas.

Sami Alkubti Almasri received the M.Sc. degree in electrical engineering from the Institute of Electrical Engineering and Information Technology, Kiel University, Kiel, Germany, in 2014, with a focus on digital communications, where he is currently pursuing the Ph.D. degree with the Chair of Information and Coding Theory, as a Research and Teaching Assistant.

His current research interests include array signal processing, in particular, position and orientation estimation using multimode antennas.

Peter Adam Hoeher (Fellow, IEEE) received the Dipl.-Ing. degree in electrical engineering from RWTH Aachen University, Aachen, Germany, in 1986, and the Dr.-Ing. degree in electrical engineering from the University of Kaiserslautern, Kaiserslautern, Germany, in 1990.

From 1986 to 1998, he was with the German Aerospace Center (DLR), Oberpfaffenhofen, Germany. From 1991 to 1992, he was on leave at AT&T Bell Laboratories, Murray Hill, NJ, USA. In 1998, he joined the University of Kiel, Kiel, Germany, where he is currently a Full Professor of electrical and information engineering. His research interests are in the general area of communication theory and applied information theory with applications in wireless radio communications, optical wireless communications, molecular communications, underwater communications, and advanced communications in power electronics.

Dr. Hoeher has been a fellow of IEEE for contributions to decoding and detection that include reliability information since 2014. He and his students received several awards and best paper awards. From 1999 to 2006, he served as an Associated Editor for the IEEE TRANSACTIONS ON COMMUNICATIONS.